Appl. Phys. A (2014) 116:1261–1269
DOI 10.1007/s00339-013-8217-y

Applied Physics A
Materials Science & Processing

A rapid synthesis/growth process producing massive ZnO nanowires for humidity and gas sensing

Nai-Feng Hsu · Tien-Kan Chung

Received: 14 October 2013 / Accepted: 19 December 2013 / Published online: 27 December 2013

Abstract We report a rapid and simple process to massively synthesize/grow ZnO nanowires capable of manufacturing massive humidity/gas sensors. The process utilizing a chemical solution deposition with an annealing process (heating in vacuum without gas) is capable of producing ZnO nanowires within an hour. Through depositing the ZnO nanowires on the top of a Pt-interdigitated-electrode/SiO_2/Si-Wafer, a humidity/gas-hybrid sensor is fabricated. The humidity sensitivity (i.e., ratio of the electrical resistance of the sensor at 11–95 % relative humidity level) is approximately 10^4. The response and recovery time with the humidity changing from 11 to 95 % directly and reversely is 6 and 10 s, respectively. The gas sensitivity (i.e., ratio of electrical resistance of the sensor under the air to vaporized ethanol) is increased from 2 to 56 when the concentration of the ethanol is increased from 40 to 600 ppm. Both the response and recovery times are less than 15 s for the gas sensor. These results show the sensor utilizing the nanowires exhibits excellent humidity and gas sensing.

1 Introduction

Chemical sensors are comprehensively used to monitor the environmental and manufacturing process in the chemical industry to ensure workplace safety [1]. Chemical sensors (or the sensing approach) have also been used in medical devices, systems, and instruments [2]. Among chemical sensors, humidity and gas sensors have developed rapidly in recent years. Researchers recently demonstrated ultra-high sensing performance with humidity and gas sensors based on ZnO, Ce_2O, TiO_2, In_2O_3 and CuO nanowires, with the performance enhancement due to the very high surface-to-volume ratio of nanowires as opposed to bulk materials [3–8]. ZnO nanowires have received considerable attention due to the excellent molecular absorption and desorption properties they lend to humidity sensors [9]. In addition, ZnO nanowires feature numerous oxygen vacancies which enhance the interaction between the ZnO nanowires and gas molecules, thus enabling an ultra-high sensitive gas sensing [10]. While ZnO nanowires have been widely used as the sensing materials for humidity and gas sensors, mass production of such sensors remains a challenge because of the difficulty in growing sufficiently large ZnO nanowires. Current synthesis and fabrication approaches include thermal evaporation [11], sputtering [12], chemical vapor deposition [13], molecular beam epitaxy [14], sol–gel [15], vapor–solid, vapor–liquid–solid [16–18], pulsed-laser deposition [19], and hydrothermal methods [20, 21]. However, the mass production of sensors requires the production of massive ZnO nanowires and the aforementioned methods are either too complicated or time consuming. Hence, this paper reports a rapid, simple, efficient, and economical approach to synthesize and grow massive ZnO nanowires using a chemical solution deposition combined with an annealing process (heating in vacuum without gas). In addition, conventional thermal oxidation usually employs an environment with oxygen to synthesize the ZnO nanowires with sufficient oxygen defect [22, 23]. In contrast to the conventional thermal oxidation, our ZnO

N.-F. Hsu (✉)
Department of General Education and Power Mechanical Engineering, Army Academy, Chung Li 32092, Taiwan
e-mail: nai-feng@hotmail.com

T.-K. Chung
Department of Mechanical Engineering,
National Chiao Tung University, Hsin-chu 30010, Taiwan

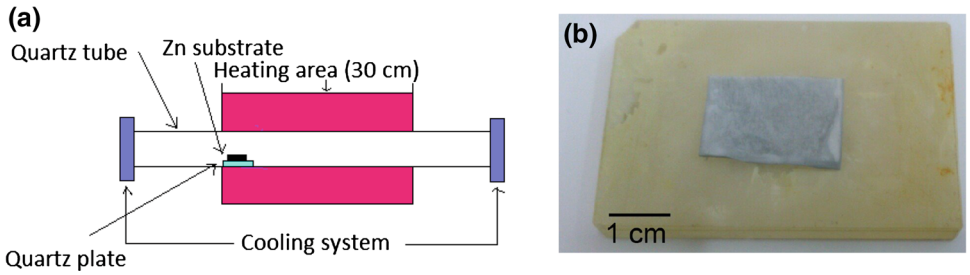

Fig. 1 **a** The illustration of the experiment setup for the synthesis/growth of the ZnO nanowires. **b** The Zinc substrate after dipped in the oxalic acid solution of 0.3 mol/L for 20 min is set on the quartz plate and ready to upload into the furnace

nanowires were grown with substantial oxygen defect on their surfaces in a vacuum through the annealing process. When oxygen defect of the ZnO nanowires is increased, the measurement sensitivity of the ZnO nanowires as gas and humidity sensing materials is significantly enhanced [24–26]. To demonstrate humidity and gas sensing capabilities, the synthesized/grown ZnO nanowires are deposited on the top of Pt-interdigitated electrodes fabricated on a SiO_2/Si-wafer as a gas and humidity sensor.

2 Experiment

2.1 Synthesis/growth Process of ZnO nanowires

Figure 1a illustrates the synthesis/growth experiment of ZnO nanowires. A metallic zinc sheet (purity 99.9 %) with a thickness of 0.5 mm and area of 3 cm^2 as the seed layer for growing the ZnO nanowires is cleaned in an ultrasonic bath with deionized water for 5 min and subsequently dipped in an oxalic acid solution of 0.3 mol/L for 20 min. The metallic Zn substrate is set on a quartz plate (as shown in Fig. 1b) placed inside a quartz furnace tube and heated from room temperature to 200 °C in air with a constant ramping rate of 70 °C/min. After this, the quartz tube is vacuumed and further heated until reaching the temperature range of 680–850 °C. Finally, the quartz tube is rapidly cooled to room temperature, producing the crystallized ZnO nanowires aggregated in powder form.

In the thermal oxidation process of the Zn substrate, the $ZnC_2O_4{\cdot}H_2O$ compound is formed when the temperature of the Zn substrate is below 190 °C. When the temperature of the Zn substrate exceeds 190 °C, the $ZnC_2O_4{\cdot}H_2O$ compound is gradually transformed into a ZnO layer [18]. The ZnO layer becomes unstable as oxygen atoms in the ZnO layer diffuse out under high temperature in a vacuum [27, 28]. The Zn atoms then interact with the diffused oxygen atoms to form ZnO nanowires. This also results in many oxygen vacancies and interstitial oxygen on the surfaces of the ZnO nanowires. Furthermore, the separation rate of the electron–hole pairs increases with oxygen vacancies and interstitial oxygen (i.e., oxygen defects) [29]. Therefore, increasing the defects on the surfaces of the ZnO nanowires enhances the sensitivity of the sensors [24–26].

2.2 Sensor fabrication

Figure 2a shows the fabricated humidity/gas-hybrid sensor. The sensor consists of ZnO nanowires as the sensing material, a Pt-interdigitated electrode as the sensing electrode, and an oxide/silicon wafer as the substrate. The process of fabricating the electrode on the sensor substrate is shown in Fig. 2b [30, 31]. The oxide layer is grown on a 20×20 mm^2 silicon wafer by thermal oxidation. The Pt-interdigitated electrode is deposited on the SiO_2/Si-wafer by e-beam evaporation and subsequently patterned by photolithography using the lift-off process. Figure 2c presents a schematic diagram of the fabricated Pt-interdigitated electrode (sixteen pairs of finger electrode). The thickness, length, and width of each Pt finger electrode are 50 nm, 12.25 mm, and 220 μm, respectively. The gap between two neighboring Pt finger electrodes is 220 μm. ZnO nanowires weighing approximately 2.4 g were dispersed in distilled water (6 ml) by sonication for 10 min. The suspension solution was then dropped onto the Pt-interdigitated electrode and dried at 180 °C in air for 3 min. After drying, the ZnO nanowires were distributed and bonded on the electrode and substrate. This configuration allows the resistance variation of the electrode caused by the humidity and gas change to be monitored. The mixed solution can produce approximately eighteen sensors. That is, our synthesis/growth process can be used to produce ZnO nanowires and the corresponding sensors on a massive scale.

To compare with our ZnO-nanowires sensor, we also fabricate a sensor using commercial ZnO particles (Shimakyu's Pure Chemicals Company, purity 99.0 %; diameter of the particle is approximately 900 nm; total weight of the particles is the same as the nanowires we used for the sensor) using the same sensor-fabrication process.

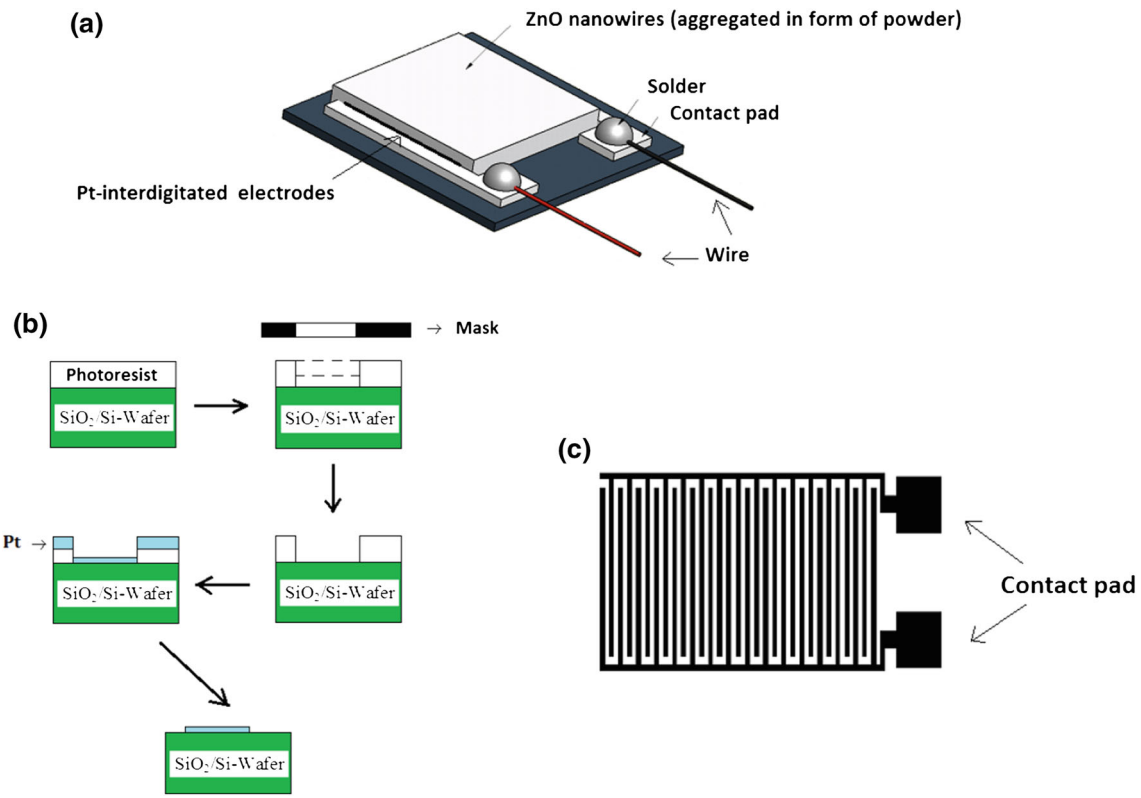

Fig. 2 **a** The illustration of the sensor. **b** The schematic diagram of fabrication process of Pt-interdigitated electrode deposited on SiO_2/Si-wafer (in *cross-sectional view*). **c** The illustration of sixteen pairs of fingers in the Pt-interdigitated electrode (in *top-view*)

2.3 Testing of humidity and gas sensing

The resistance variations of the sensor electrode under changes to humidity and gas concentrations were measured using a computerized Agilent U2722A multimeter.

In humidity testing, the amount of water vapor present in a gas is measured and indicated in terms of relative humidity (RH) which is the ratio of the partial pressure of water vapor present in a gas to the saturated vapor pressure of the gas at a given temperature. According to the design and configuration of our sensors, the RH is measured by monitoring resistance variation of the sensor's electrode. The various RH levels used for testing are controlled using super-saturated aqueous solutions of different salts in a sealed glass vessel at room temperature (26 °C). The salts used include LiCl, $MgCl_2$, $Mg(NO_3)_2$, NaCl, KCl, and KNO_3, yielding respective RH levels of 11, 33, 54, 75, 85, and 95 % [29]. These RH levels were independently monitored using a standard hygrometer. AC 1 V was applied at a frequency of 60 Hz. The operation temperature was controlled at 26 °C when the resistance of the humidity sensor is measured.

When a ZnO-nanowire-based sensor detects a gas such as vaporized ethanol, the surface resistance of the electrode of the sensor changed [32, 33]. Therefore, the fabricated sensor (i.e., the sensor with ZnO nanowires) is capable of sensing/detecting the vaporized ethanol. The gas sensing test used vaporized ethanol (prepared through heating an ethanol solution at 220 °C [34–36]) with concentrations ranging from 40 to 600 ppm. As different concentrations of ethanol were detected by the sensor, the resistance variation of the sensor's electrode was monitored using the computerized multimeter.

The testing of the ZnO-particles-based sensor is the same as the ZnO-nanowire-based sensor.

3 Results and discussion

Figure 3a, b, respectively, shows photographs of ZnO nanowires (aggregated in form of powder) synthesized/grown on the zinc substrate set on the quartz plate and the Pt-interdigitated electrode fabricated on the SiO_2/Si-wafer. The ZnO nanowires removed from the zinc substrate are deposited on the Pt-interdigitated-electrode/SiO_2/Si-wafer, as shown in Fig. 3c. Subsequently, the electrode pads are connected with electrical wires to complete the humidity/gas-hybrid sensor.

Figure 4 shows the XRD pattern of the ZnO nanowires growth at an annealing temperature of 800 °C in a vacuum.

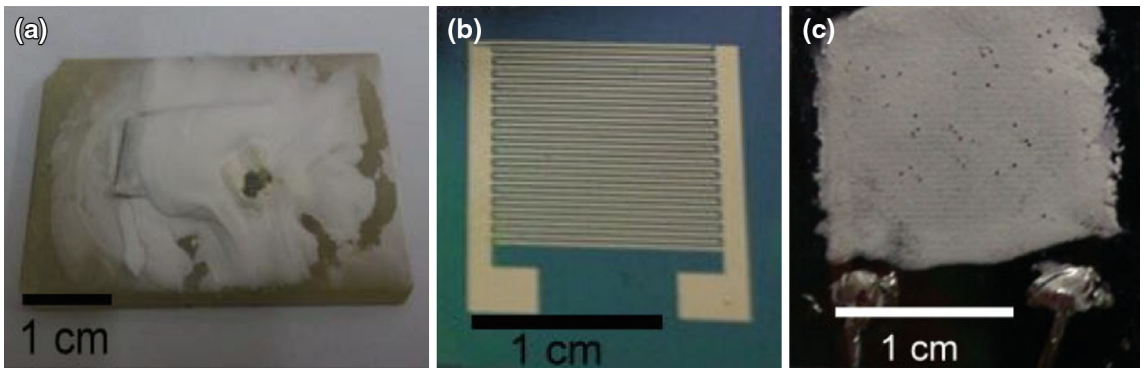

Fig. 3 The photograph of **a** the ZnO nanowires (aggregated in the form of powder) synthesized/grown on the Zinc substrate set on the quartz plate. **b** The Pt-interdigitated electrode with sixteen pairs of fingers fabricated on the SiO_2/Si-wafer. **c** The ZnO nanowires deposited on the Pt-interdigitated-electrode/SiO_2/Si-wafer as the humidity/gas-hybrid sensor

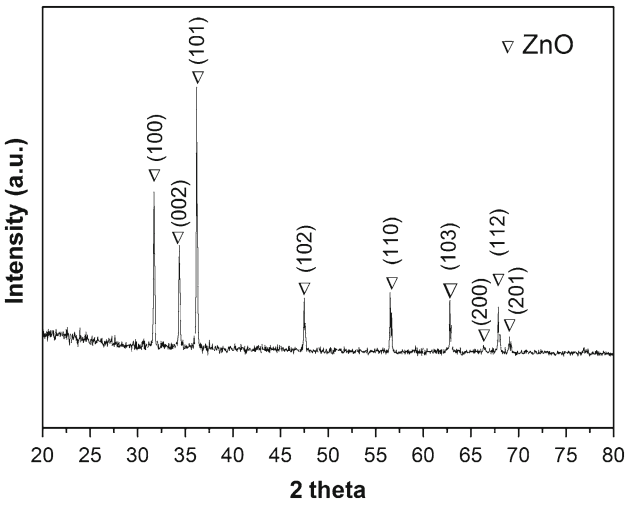

Fig. 4 The XRD pattern of ZnO nanostructures grown at annealing temperature of 800 °C in vacuum

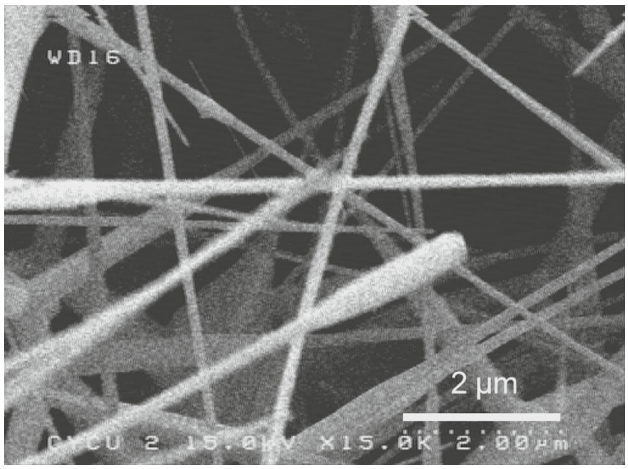

Fig. 5 The SEM image of the ZnO nanowires grew at annealing temperature of 800 °C

According to the XRD reference peaks of ZnO, the peaks indexed to (100), (002), (101), (102), (110), (103), (200), (112), and (201) crystal plane which we obtained in the XRD pattern are, respectively, located at $2\theta = 31.8°$, 34.4°, 36.3°, 47.5°, 56.6°, 62.9°, 66.4°, 67.9°, and 69.1°. This shows the grown ZnO crystalline displays a wurtzite structure which is consistent with the standard ZnO bulk crystal (JCPDS No 36-1451) [37].

Figure 5 shows an SEM image of ZnO nanowires grown at an annealing temperature of 800 °C. The average length and diameter of the ZnO nanowires is approximately 10 μm and 150 nm, respectively. Figure 6a, b, respectively, shows TEM and HR-TEM images of a single ZnO nanowire and a certain point on a single ZnO nanowire. In Fig. 6b, the HR-TEM image indicates that the ZnO nanowires growth direction is perpendicular to the lattice planes. The lattice spacing of about 0.26 nm is in agreement with the interplanar spaces of (002) of wurtzite structured ZnO [38]. That is, the ZnO nanowires we synthesized/grew exhibit a wurtzite structure. Furthermore, Fig. 6c shows the corresponding elected-area electron diffraction (SAED) result of the ZnO nanowire shown in Fig. 6a. When the SAED result is compared with other results from the literature [39], we conclude that the synthesized/grown ZnO nanowires take the form of a single crystalline with a wurtzite structure.

Figure 7 shows the Raman scattering spectra of the ZnO nanowires grown at an annealing temperature of 800 °C. The Raman scattering spectra were taken with an exposure time of 60 s from a 0.1 mm slit excited by a laser light ($\lambda = 514.5$ nm). The Raman spectra reveal that five peaks appearing at 379, 413, 437, 579, and 587 cm^{-1} correspond to ZnO NWs. The peaks appearing at 378, 412, 436, 579, and 587 cm^{-1} are, respectively, assigned to A_1-TO, E_1-TO, E_2-high, A_1-LO, and E_1-LO of the bulk ZnO [40, 41]. The sharp E_2-high mode located at 437 cm^{-1} is an intrinsic characteristic of a Raman active mode of wurtzite

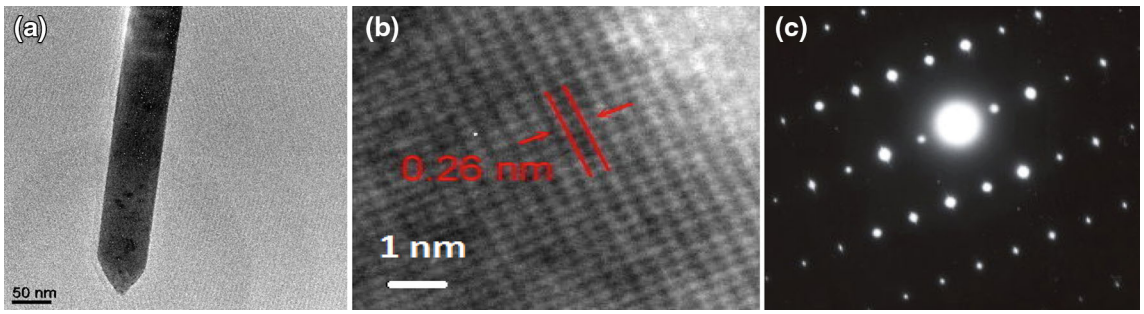

Fig. 6 **a** TEM image of a single ZnO nanowire taken at a low magnification. **b** HR-TEM image taken at a certain point of the single ZnO nanowires in **a**. **c** The diffraction pattern of the ZnO nanowires in the corresponding area selected in **a**

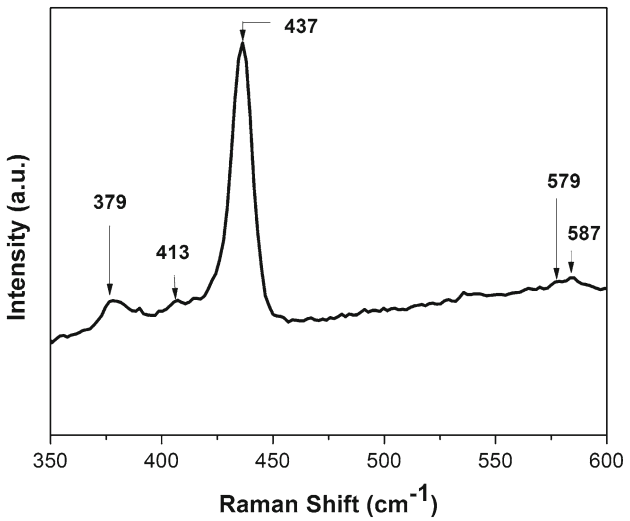

Fig. 7 The Raman scattering spectra of the ZnO nanowires grown at annealing temperature of 800 °C

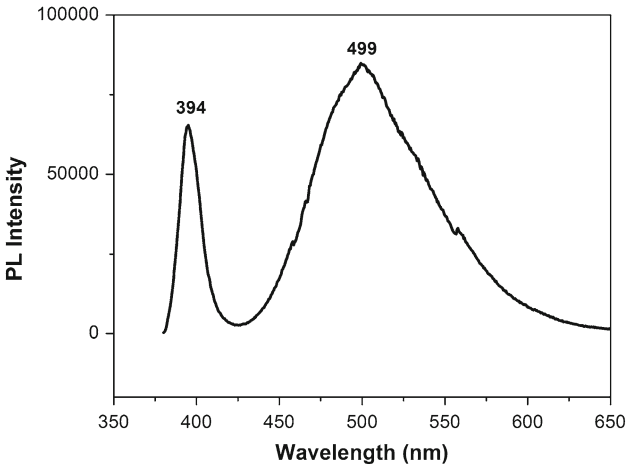

Fig. 8 The PL spectrum of the ZnO nanowires grown at annealing temperature of 800 °C

hexagonal ZnO [42]. According to the Raman spectra, the E_2-high pattern has a width of 25 cm^{-1} and no obvious peak appears at 587 cm^{-1}, which corresponds to the E_1-LO mode of ZnO crystals associated with oxygen deficiency and interstitial zinc atoms. This finding shows the synthesized/grown ZnO nanowires are of high quality [43].

Figure 8 shows the room temperature photoluminescence (PL) spectrum of the ZnO nanowires grown at an annealing temperature of 800 °C. The PL spectrum was recorded using a He–Cd ($\lambda = 260$ nm) laser as the illumination source. The ultra-violet (UV) near band edge emission peak appears near 394 nm, and the appearance of deep-level emissions at approximately 499 nm indicates the presence of oxygen vacancies. In Fig. 8, the full width at half maximum (FWHM) of the UV emission peak is 13 nm. The narrow FWHM of the UV emission peak indicates that high quality ZnO nanowires [44] are synthesized through our annealing process in a vacuum. Furthermore, the UV and green emission is attributed to the radiative recombination of an excited electron in the conduction band with a hole in valence band and the recombination of a photogenerated hole with a defect's ionized charge, respectively [45]. Thus, when the intensity of the UV emission is lower than the green emission, a higher concentration of oxygen vacancies is formed on the surfaces of nanostructures [25, 46–48]. Thus, nanostructures with a higher surface-to-volume ratio than their corresponding bulk materials are seen as containing much more surface oxygen vacancies, resulting in the intensity of the UV emission lower than green emission [48]. In Fig. 8, we observed a narrow FWHM of the UV emission peak and the intensity of the UV emission was lower than the green emission. Due to this, our grown ZnO nanowires have excellent crystal quality with lots of oxygen vacancies on the surfaces of the nanowires.

For humidity sensing, the measured resistance variation of the humidity sensor at different RH is shown in Fig. 9a. The resistance of the sensor at 11, 33, 54, 75, 85, and 95 % RH is, respectively, 1,125, 616, 150, 12.8, 2.7, and 0.1 MΩ. Experimental results indicate that the measured resistance decreases exponentially as RH is increased

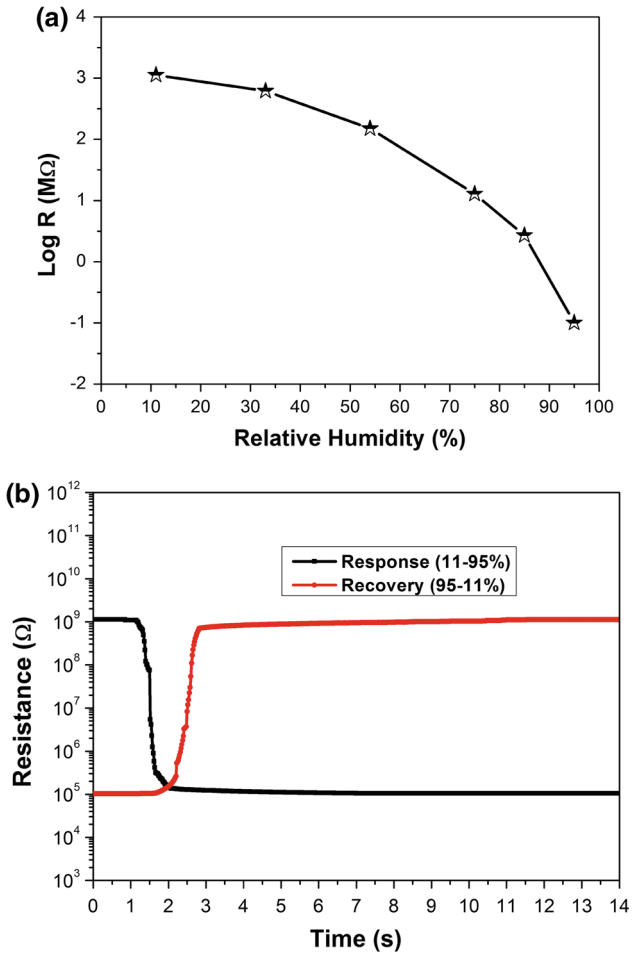

Fig. 9 **a** The resistance variation of the humidity sensor at different RH. **b** The response and recovery time of the sensor in one testing cycle

because of the increased absorption of water molecules by the ZnO nanostructures. This same phenomenon was observed in other studies [49]. In a lower humidity testing environment (i.e., reduced RH), fewer water molecules are adsorbed on the surfaces of the nanowires because the water molecules fail to form a complete water membrane to cover the surfaces of the nanowires. Thus, electrolytic conduction does not dominate the absorption mechanism in this phase and resistance is relatively high. However, in tests with a higher RH, the water membrane is completely formed on the surfaces of the nanowires of the sensor. This accelerates the transfer of H^+ or H_3O^+ resulting in relatively low resistance [50]. Therefore, the resistance of the sensor is decreased when the RH is increased, providing a linear-operation region as the sensor. Furthermore, according to the results shown in Fig. 9a, the resistance variation of the sensor at different RH levels (i.e., in humidity sensing) exceeds four orders of magnitude. This indicates the humidity sensitivity of the sensor (i.e., the ratio of the electrical resistance of the sensor at 11–95 % RH) is 1.125×10^4. The electron–hole pair separation rate can be enhanced by the presence of oxygen vacancies and interstitial oxygen defects [29]. Hence, this high degree of sensitivity may be mainly due to the many defects on surfaces of the ZnO nanowires. In addition to the resistance variation under different degrees of humidity, Fig. 9b shows the response time (from 11 % RH to 95 % RH) and recovery time (from 95 % RH to 11 % RH) of the sensor in one testing cycle of 6 and 10 s, respectively. These rapid responses may be attributed to the significantly enhanced absorption and desorption processes of water molecules caused by the increased surface-to-volume ratio of the structure of the ZnO nanowires [51].

When we consider the ZnO-nanowires layer deposited on the electrode of the sensor as a continuous thin film with two parallel surfaces (i.e., top and bottom), the water molecule is much more easily absorbed by the top surface than the bottom surface because the water molecule is in direct contact with the top surface. Thus, the resistance of the top surface is lower than that of the bottom surface and the current on the thin film can easily pass through the top surface. Therefore, the resistance quickly decreases and reaches a steady state in the response process. On the contrary, desorption of the water molecules from the lower surface is more difficult and a longer recovery time is needed. The absorption and desorption phenomena we observed are similar to those reported elsewhere [52], and these results indicate that sensors using the ZnO nanowires as the sensing material perform well in humidity sensing.

For the gas sensing test, Fig. 10 shows the measured electrical resistance of the sensors tested using different concentrations of vaporized ethanol. At an operating temperature of 220 °C, the measured resistance at concentrations of 0, 40, 80, 160, 400, and 600 ppm is 5.68, 2.74, 2.29, 1.5, 0.59, and 0.1 MΩ, respectively. According to these results, we found resistance variation of the ZnO-nanowire-based sensor decreases when the concentration of the vaporized ethanol increases from 40 to 600 ppm. In addition, Fig. 10b indicates the gas sensitivity of the ZnO-nanowire-based sensor (i.e., the ratio of the measured electrical resistance under the air to the vaporized ethanol) increases significantly from 2 to 56 when the concentration of the vaporized ethanol is increased from 40 to 600 ppm. These phenomena were comparable results from other studies [53]. From Fig. 10a, we observe that, when the ZnO-nanowire-based sensor detects vaporized ethanol at a concentration below 40 ppm, the measured resistance variation decreases rapidly. This indicates the ZnO-nanowire-based sensor has an excellent gas sensing capability for detecting vaporized ethanol at low concentrations. When the gas concentration exceeds 160 ppm, the measured resistance variation slowly decreases. This is

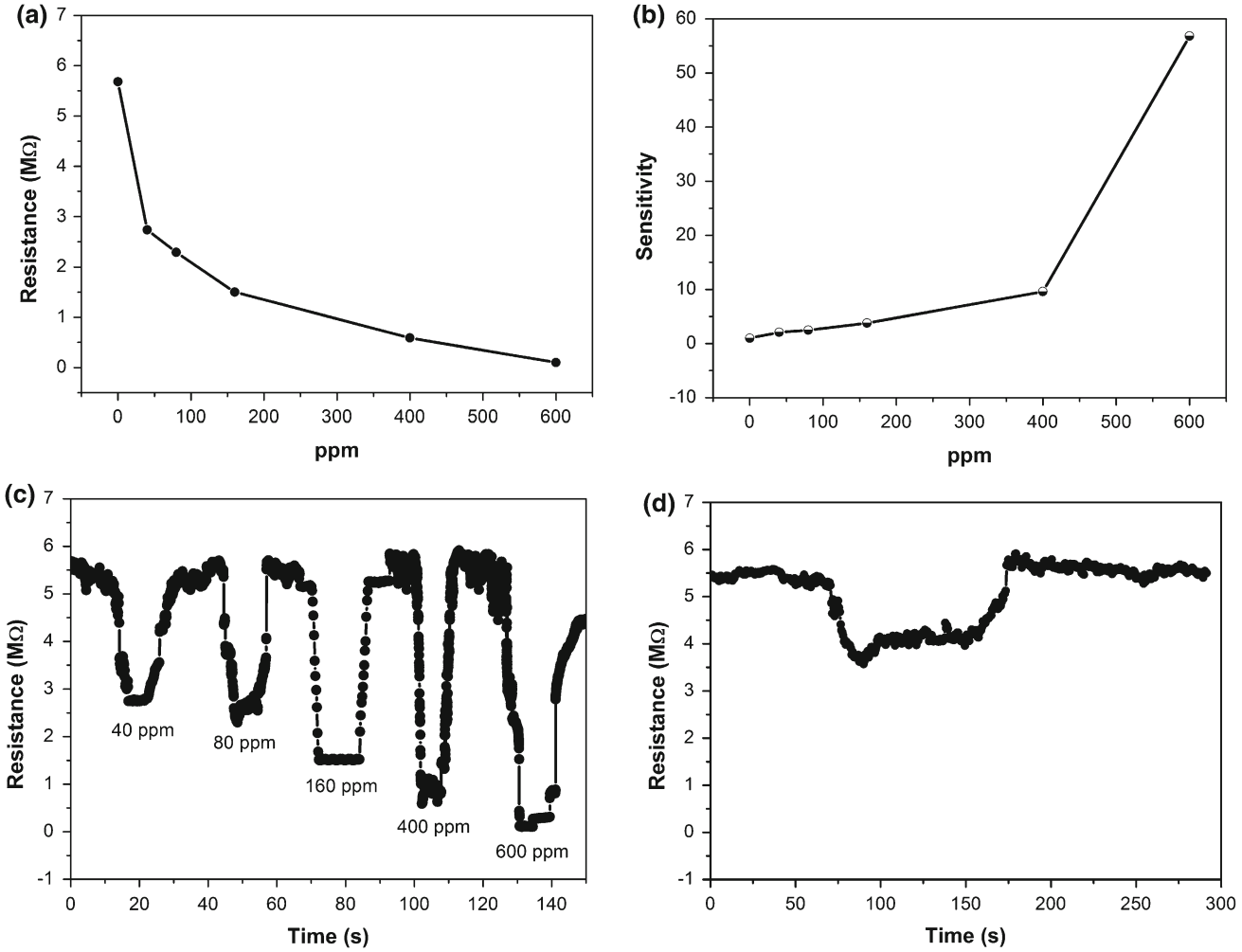

Fig. 10 **a** The resistance, **b** the sensitivity, **c** the response and recovery time of the ZnO-nanowire-based sensor tested using ethanol with different concentration at 220 °C. **d** The response and recovery time of the ZnO-particles-based sensor tested using the ethanol with a concentration of 600 ppm at 220 °C

attributed to the ZnO nanostructures being saturated with vaporized ethanol. The response and recovery times are determined when the time reached 90 % of the steady-state signal [54]. The response (from air to a sample gas) and the recovery (from a sample gas to air) times are found to be less than 15 s (Fig. 10c). Thus, we can conclude the synthesized/grown ZnO nanowires can be used as the sensing material to produce highly sensitive and reliable gas sensors. Furthermore, we compared the gas-testing results of ZnO-nanowire-based sensor (refer Fig. 10c with ZnO-particles-based sensor (refer Fig. 10d). In Fig. 10c, d, the response and recovery time of the ZnO-nanowire-based and ZnO-particles-based sensor is approximately 15 and 125 s, respectively. Moreover, through calculating from the Fig. 10c, d, the gas sensitivity of the ZnO-nanowire-based and ZnO-particles-based sensor tested using an ethanol with a concentration of 600 ppm at operating temperature of 220 °C is approximately 56 and 1.6, respectively. The estimated surface-to-volume ratio of the ZnO nanowires and ZnO particles is 26.9×10^6 and 6.7×10^6 m^{-1}, respectively (note: we assume the ZnO nanowire and particle are cylindrical and spherical type for estimation, respectively). Therefore, according to the comparison of sensors' response/recovery times and sensitivity and ZnO materials' surface-to-volume ratio, we can conclude that the sensitivity of ZnO-nanowire-based sensor is much better than ZnO-particles-based sensor and this is attributed to the larger surface-to-volume ratio of our nanowires than the commercial ZnO particles used by the sensor for the gas sensing [26]. Finally, the sensors were continuously subjected to humidity and gas sensing tests over the course of a month. Only a slight fluctuation (less than 3 %) was found in the results for the resistance variation measurements, indicating that the sensors have

excellent long-term stability. That is, the fabricated ZnO-nanowire-based sensors provide reliable and durable humidity and gas sensing.

4 Conclusions

A rapid, simple, and novel process utilizing a chemical solution deposition method with an annealing approach is used to synthesize and grow ZnO nanowires on a massive scale. Using semiconductor manufacturing technology (i.e., silicon processing), the resulting massive synthesized/grown ZnO nanowires can be applied for the mass production of humidity, gas, and humidity/gas-hybrid sensors. The humidity sensitivity of the resulting sensor (i.e., the ratio of the electrical resistance of the sensor at 11–95 % RH) is approximately 10^4. The gas sensitivity of the sensor (i.e., the ratio of measured electrical resistance under the air to the vaporized ethanol) increased from 2 to 56 when the concentration of the vaporized ethanol was increased from 40 to 600 ppm. The humidity/gas-hybrid sensors also exhibit rapid response and recovery characteristics. These results indicate the sensor using the synthesized/grown ZnO nanowires has excellent humidity and gas sensing capabilities.

Acknowledgments The authors would like to thank the National Science Council of the Republic of China, Taiwan, for financially supporting this research under Contract No. NSC 101-2218-E-539-001 and NSC 102-2623-E-539-001-ET. The authors also thank Mr. Chieh-Min Wang in National Chiao Tung University, Taiwan for the electrode preparation and TEM/HR-TEM characterization.

References

1. N. Yamazoe, Sens. Actuators B **5**, 7 (1991)
2. A. Tételin, C. Pellet, C. Laville, G. N'Kaoua, Sens. Actuators B **91**, 211 (2003)
3. S.P. Chang, S.J. Chang, C.Y. Lua, M.J. Li, C.L. Hsu, Y.Z. Chiou, T.J. Hsueh, I.C. Chen, Superlattices Microstruct. **47**, 772 (2010)
4. X.Q. Fu, C. Wang, H.C. Yu, Y.G. Wang, T.H. Wang, Nanotechnology **18**, 145503 (2007)
5. L. Francioso, A.M. Taurino, A. Forleo, P. Siciliano, Sens. Actuators B **130**, 70 (2008)
6. C. Li, D.H. Zhang, X.L. Liu, S. Han, T. Tang, J. Han, C.W. Zhou, Appl. Phys. Lett. **82**, 1613 (2003)
7. G. Wang, Q. Wang, W. Lu, J. Li, J. Phys. Chem. B **110**, 22029 (2006)
8. D. Li, J. Hu, R. Wu, J.G. Lu, Nanotechnology **21**, 485502 (2010)
9. Y. Chen, D.M. Bagnall, H. Koh, K. Park, K. Hiraga, Z. Zhu, T. Yao, J. Appl. Phys. **84**, 3912 (1998)
10. L.S. Mende, J.L. MacManus-Driscoll, Mater. Today **10**, 40 (2007)
11. S. Park, S. An, C. Jin, C. Lee, Appl. Phys. A **108**, 35 (2012)
12. K.K. Kim, J.H. Song, H.J. Jung, W.K. Choi, S.J. Park, J.H. Song, J. Appl. Phys. **87**, 3573 (2000)
13. D. Zhang, S. Chava, C. Berven, S.K. Lee, R. Devitt, V. Katkanant, Appl. Phys. A **100**, 145 (2010)
14. B.S. Kang, Y.W. Heo, L.C. Tien, D.P. Norton, F. Ren, B.P. Gila, S.J. Pearton, Appl. Phys. A **80**, 1029 (2005)
15. S.E. Ahn, H.J. Ji, K. Kim, G.T. Kim, C.H. Bae, S.M. Park, Y.K. Kim, J.S. Ha, Appl. Phys. Lett. **90**, 153106 (2007)
16. C.K. Xu, M. Kim, S.Y. Chung, D.E. Kim, Solid State Commun. **132**, 837 (2004)
17. E.W. Petersen, E.M. Likovich, K.J. Russell, V. Narayanamurti, Nanotechnology **20**, 405603 (2009)
18. N.F. Hsu, M. Chang, Mater. Chem. Phys. **135**, 112 (2012)
19. L.C. Tien, S.J. Pearton, D.P. Norton, F. Ren, J. Mater. Sci. **43**, 6925 (2008)
20. L. Wu, Y. Wu, J. Mater. Sci. **42**, 406 (2007)
21. G. Amin, M.O. Sandberg, A. Zainelabdin, S. Zaman, O. Nur, M. Willander, J. Mater. Sci. **47**, 4726 (2012)
22. M.R. Khanlary, V. Vahedi, A. Reyhani, Molecules **17**, 5021 (2012)
23. D. Somvanshi, S. Jit, Adv. Mater. Res. **585**, 124 (2012)
24. L. Li, K. Yu, J. Wu, Y. Wang, Z. Zhu, Cryst. Res. Technol. **45**, 539 (2010)
25. T.J. Hsueh, Y.W. Chen, S.J. Chang, S.F. Wang, C.L. Hsu, Y.R. Lin, T.S. Lin, I.C. Chen, Sens. Actuators B **125**, 498 (2007)
26. C.M. Chang, M.H. Hon, I.C. Leu, Sens. Actuators B **151**, 15 (2010)
27. J. Zhang, N. Li, Oxid. Met. **63**, 353 (2005)
28. M. Ohring, *The Materials Science of Thin Films*, 2nd edn. (Academic Press, San Diego, 2002)
29. Q. Qi, T. Zhang, Q. Yu, R. Wang, Y. Zeng, L. Liu, H. Yang, Sens. Actuators B **133**, 638 (2008)
30. T.K. Chung, G.P. Carman, K.P. Mohanchandra, Appl. Phys. Lett. **92**, 112509 (2008)
31. T.K. Chung, S. Keller, G.P. Carman, Appl. Phys. Lett. **94**, 132501 (2009)
32. P. Feng, Q. Wan, T.H. Wang, Appl. Phys. Lett. **87**, 213111 (2005)
33. J.Q. Xu, Y.P. Chen, Y.D. Li, J.N. Shen, J. Mater. Sci. **40**, 2919 (2005)
34. Y. Lv, L. Guo, H. Xu, X. Chu, Physica E **36**, 102 (2007)
35. S. Santra, P.K. Guha, S.Z. Ali, P. Hiralal, H.E. Unalan, J.A. Covington, G.A.J. Amaratunga, W.I. Milne, J.W. Gardner, F. Udrea, Sens. Actuators B **146**, 559 (2010)
36. J. Yi, J.M. Lee, W.I. Park, Sens. Actuators B **155**, 264 (2011)
37. J. Lv, W. Gong, K. Huang, J. Zhu, F. Meng, X. Song, Z. Sun, Superlattices Microstruct. **50**, 98 (2011)
38. S. Ma, R. Li, C. Lv, W. Xu, X. Gou, J. Hazardous Mater. **192**, 730 (2011)
39. S.P. Chang, S.J. Chang, C.Y. Lu, M.J. Li, C.L. Hsu, Y.Z. Chiou, T.J. Hsueh, I.C. Chen, Superlattices Microstruct. **47**, 772 (2010)
40. N. Ashkenov, B.N. Mbenkum, C. Bundesmann, V. Riede, M. Lorenz, D. Spemann, E.M. Kaidashev, A. Kasic, M. Schubert, M. Grundmann, G. Wagner, H. Neumann, V. Darakchieva, H. Arwin, B. Monemar, J. Appl. Phys. **93**, 126 (2003)
41. C.A. Arguello, D.L. Rousseau, S.P.S. Porto, Phys. Rev. **181**, 1351 (1969)
42. J.J. Wu, S.C. Liu, J. Phys. Chem. B **106**, 9546 (2002)
43. H.C. Hsu, H.M. Cheng, C.Y. Wu, H.S. Huang, Y.C. Lee, W.F. Hsieh, Nanotechnology **17**, 1404 (2006)
44. X. Zhang, L. Wang, G. Zhou, Rev. Adv. Mater. Sci. **10**, 69 (2005)
45. K. Vanheusden, W.L. Warren, C.H. Seager, D.R. Tallant, J.A. Voigt, J. Appl. Phys. **79**, 7983 (1996)
46. M.H. Huang, S. Mao, H. Feik, H. Yan, Y. Wu, H. Kind, E. Weber, R. Russo, P. Yang, Science **292**, 1897 (2001)
47. C.H. Hung, W.T. Whang, Mater. Chem. Phys. **82**, 705 (2003)
48. C. Xu, M. Kim, S. Chung, D.E. Kim, Solid State Commun. **132**, 837 (2004)
49. B.M. Kulwicki, J. Am. Ceram. Soc. **74**, 697 (1991)
50. F.M. Ernsberger, J. Am. Ceram. Soc. **66**, 747 (1983)

51. W. Wang, Z. Li, L. Liu, H. Zhang, W. Zheng, Y. Wang, H. Huang, Z. Wang, C. Wang, Sens. Actuators B **141**, 404 (2009)
52. Z. Zhang, C. Hu, Y. Xiong, R. Yang, Z.L. Wang, Nanotechnology **18**, 465504 (2007)
53. J.X. Wang, X.W. Sun, Y. Yang, H. Huang, Y.C. Lee, O.K. Tan, L. Vayssieres, Nanotechnology **17**, 4995 (2006)
54. N.V. Hieu, N.D. Chien, Phys. B **403**, 50 (2008)